RSC Advances

PAPER

View Article Online
View Journal | View Issue

Cite this: *RSC Adv.*, 2022, **12**, 32552

Biomass-derived nano-laminated Ti_3SiC_2 MAX phase

Changwan Nou,[a] Byeong Geun Kim,†*[b] Soo-Young Suk[b] and Soon-Mok Choi †*[a]

Received 27th September 2022
Accepted 20th October 2022

DOI: 10.1039/d2ra06078g

rsc.li/rsc-advances

Carbide-based MAX phases, titanium silicon carbide (Ti_3SiC_2), were synthesized with Ti, Si, and C elements using a sintering process. Eggshell membranes, which have been generally dumped as domestic wastes, were used as carbon sources in starting materials. After a sintering process at 1500 °C, Ti_3SiC_2 phases were mainly formed with a few secondary phases such as $TiSi_2$ and TiC_x. The formation and extinction of secondary phases were influenced by the quantities of Si contents in starting materials, which also affected the peak shifts of the Ti_3SiC_2 phase in X-ray diffraction spectra. The possible mechanism of this phenomenon was proposed, and the thermoelectric properties of products were also investigated.

Introduction

The ternary carbides and nitrides, so-called MAX phases, have received attention because of their unique properties.[1–3] They consist of early transition metal (M), elements of 13–16 families (A), and the carbon and/or nitrogen (X): $M_{n+1}AX_n$.[1–3] MAX phases have both metallic (good machinability and thermal and electrical conductivities) and ceramic properties (good thermal resistance and chemical resistance). Therefore, they are utilized in various applications such as nuclear,[4] energy,[5] filters,[6] and heating elements.[1] Moreover, they can transform to two-dimensional early transition metal carbides and carbonitrides, called MXenes, using a selected etching process of 'A' elements.[7–10] MXenes have the general formula of $M_{n+1}X_nT_x$ (n = 1–3); M and T_x indicate the early transition metals and surface terminations, respectively.[7–10] X represents carbon and/or nitrogen. MXenes are excellent candidates for applications in energy storage (ion batteries and supercapacitors *etc.*) and energy conversions (photovoltaic and thermoelectric devices *etc.*).[7–10]

MAX phases are mostly prepared using a sintering process such as a conventional reactive process,[11] hot-press,[12,13] and spark plasma sintering (SPS)[14] at high temperatures. In most processes, commercial carbon materials such as active carbon[12] and graphite[13] were used as carbon sources. Eggs have been most frequently consumed throughout the world. Hence, massive eggshell membranes are produced every day, which are thrown in the garbage. We think research about their recycling is meaningful in terms of the eco-environment. Recently, research on the transformation of biomass to functional inorganic materials has been reported.[15–18] Thus, we selected eggshell membranes as carbon sources for synthesizing MAX phases (Ti_3SiC_2) in this study.

Experimental

Eggs were purchased from a nearby grocery store. Eggshell membranes were detached from eggs by soaking them in a hydrochloric acid (HCl, 9.9%) solution. After egg yolks and whites in eggs were removed, eggshell membranes were subjected to an ultra-sonication in ethanol (99.9%) solution for 30 min. They were sufficiently dried at 70 °C using an oven for 30 min.

After thermal annealing at 900 °C with a tube furnace for 1 h under an argon (99.999%) gas atmosphere, they were lightly ground in an agate mortar and pestle by hand. Then, a planetary milling was performed for 1 h at 3000 rpm. As a result, a dark gray powder was obtained.

Ti (<45 μm, 99.98%), Si (325 mesh, 99%), and carbonized-eggshell membranes were in a molar ratio of 3 : 1.2 : 2, 3 : 1.4 : 2, and 3 : 1.6 : 2. They were named as TS1.2C, TS1.4C, and TS1.6C, respectively. The mixing process was performed with 8 zirconia balls in a zirconia jar at 300 rpm using a planetary ball mill. The mixed powder weighing 1 g was placed in a graphite mold (10 ⌀) and then was pressed to form pellets using spark plasma sintering (SPS) equipment. The working pressure, temperature, and duration time were 50 MPa, 900 °C, and 5 min, respectively. The fabricated pellets were thermally annealed at 1500 °C using a tube furnace for 4 h in an argon (99.999%) gas atmosphere. After the annealing process with a heating rate of 4 °C min^{-1}, the furnace was slowly cooled to room temperature. The whole preparation process of the MAX phases is shown in Fig. 1(a).

The microstructural, morphological, and composition analyses of specimens were conducted using X-ray diffraction (XRD,

[a]*School of Energy Materials Chemical Engineering, Korea University of Technology and Education, Cheonan-si 31253, Korea. E-mail: smchoi@koreatech.ac.kr*

[b]*Research Development Division, Gyeongbuk Institute of IT Convergence Industry Technology, Gyeongsan-si 38463, Korea. E-mail: bgkim305@gmail.com*

† These authors contributed equally to this work.

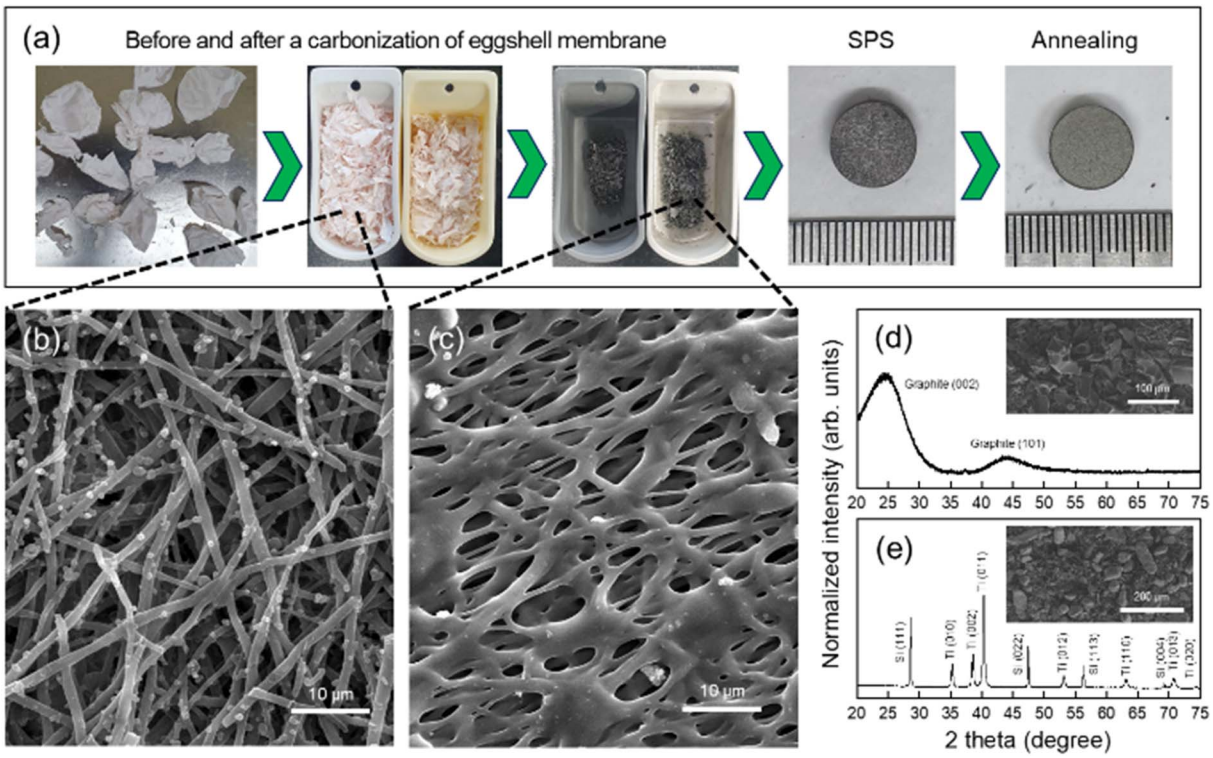

Fig. 1 (a) Schematic of all processes for preparing MAX phases. SEM images of eggshell membranes (b) before and (c) after carbonization. XRD patterns and SEM images (insets) of (d) as-carbonized eggshell membranes and (e) mixed powders before preparing pellets for SPS process.

Malvern Panalytical, UK) and two scanning electron microscopes (SEM, JEOL, Japan/EMCRAFTS, Korea) equipped with energy dispersive spectroscopy (EDS), respectively. The density of the products was measured using the Archimede's method. Their thermoelectric properties were determined by temperature differential and four-probe methods using commercial equipment (RZ2000li, Ozawa Science Co., Japan) in the temperature range from room temperature to about 590 °C under an Ar (99.999%) gas atmosphere.

As-exfoliated eggshell membranes have a net-liked shape, composed of many fibers with an average diameter of 1.36 μm (Fig. 1(b)). Several elements were found in the EDS mapping analyses: C (62.6 at%), N (19.6 at%), O (15.8 at%), and S (1.3 at%). When eggshell membranes were thermally treated at 900 °C, their weight was decreased to about 76%. The compositions also changed into C (88.6 at%), N (7.8 at%), and O (3.5 at%). In addition, the traces (less than 0.1 at%) such as Cl, S, and Ca were detected in all EDS analyses. These results were due to the thermal decomposition of organic components at high temperatures.

The carbonized eggshell membranes have broad XRD patterns (Fig. 1(d)), indicating that they were nearly amorphous or nano-crystalline. Fig. 1(e) shows the XRD pattern of the mixed-powders with Ti, Si, and carbonized eggshell membranes before the SPS process. All peaks were indexed with Si (ICSD no. 426975) and Ti (ICSD no. 192331) phases, not C-related crystalline peaks. The inner SEM images in Fig. 1(d) and (e) show the morphologies of as-carbonized eggshell membranes and mixed powders in each process.

Fig. 2 shows low-(inner images) and high-magnification SEM images of TS1.2C, TS1.4C, and TS1.6C after thermal annealing. The unique laminated morphologies of MAX phases are clearly observed in all products. Moreover, the yellow arrow in Fig. 2(b) presents that step growth of Ti_3SiC_2 was carried out.[19,20]

To further verify the formation of Ti_3SiC_2 phases, XRD analyses were performed (Fig. 3). The XRD patterns show that Ti_3SiC_2 phases were mainly formed with secondary phases such as $TiSi_2$, Ti_5Si_3, and TiC_x. The peaks were indexed with Ti_3SiC_2 (ICSD no. 25762), $TiSi_2$ (ICSD no. 96029), Ti_5Si_3 (ICSD no. 652424), and $Ti_{5.73}C_{3.72}$ (TiC_x, ICSD no. 18494). TSC, TS53, TS12, and TC in Fig. 3 indicate Ti_3SiC_2, Ti_5Si_3, $TiSi_2$, and TiC_x phases, respectively. From the results of XRD analyses, the possible reaction mechanism during the sintering process is described as follows:[21]

$$\mathrm{Ti(s)} + x\mathrm{C(s)} \rightarrow \mathrm{TiC}_x\mathrm{(s)} \quad (1)$$

$$\mathrm{Ti(s)} + y\mathrm{Si(s)} \rightarrow \mathrm{Ti–Si_{rich}(l)} \quad (2)$$

$$\mathrm{TiC}_x\mathrm{(s)} + \mathrm{Ti–Si_{rich}(l)} \rightarrow \mathrm{Ti_3SiC_2(s)} + \mathrm{TiSi_2(s)} + \mathrm{Ti_5Si_3(s)} + \mathrm{TiC}_x\mathrm{(s)} \quad (3)$$

According to the quantities of Si contents in the starting materials, the XRD patterns of secondary phases were slightly changed. When Si contents were increased, the intensities of $TiSi_2$ and TiC_x peaks were increased and decreased, respectively (Fig. 3(b)). It is known that excess Si is needed for the increase of

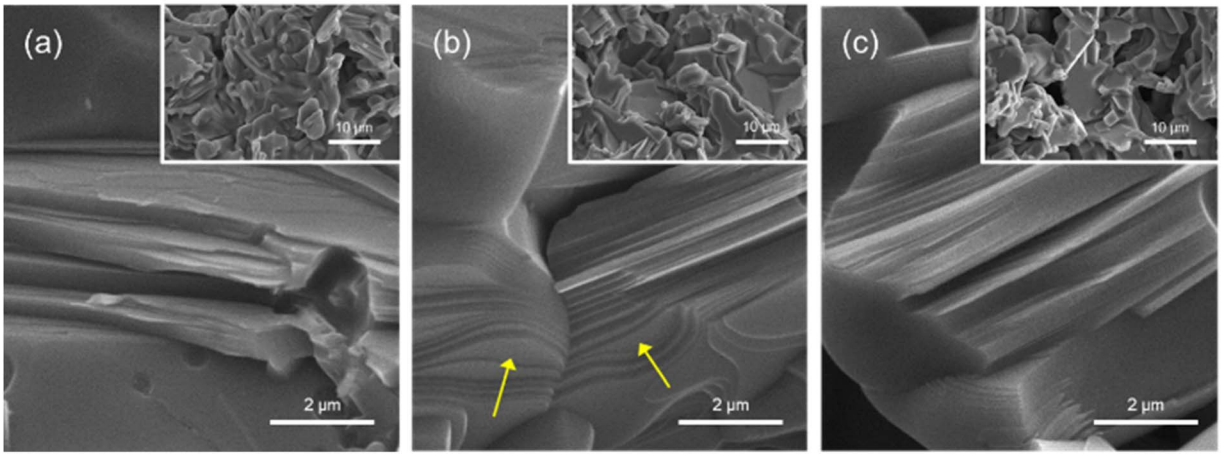

Fig. 2 SEM images of (a) TS1.2C, (b) TS1.4C, and (c) TS1.6C.

the newly-formed Ti_3SiC_2 phase because the melted Si can partially be evaporated during the fabrication process at high temperatures.[21] Inset of Fig. 3(a) presents the intensity variations of the main peak of the Ti_3SiC_2 phase at about 39°. When Si content is increased, it shows a tendency to increase the intensities of the products. This phenomenon was also found for the second peak (at about 42.7°) of the Ti_3SiC_2 phase. The reason may be that excess Si induces the formation of both Ti_3SiC_2 and Ti-based secondary phases, such as $TiSi_2$.

In addition, we found one interesting pattern in enlarged XRD peaks in Fig. 3(b). The peaks of the Ti_3SiC_2 phase were shifted to the higher position with the increase in Si contents (Fig. 4), while the peaks of secondary phases were not changed. This indicates that the lattice constants and the size of the unit cells were decreased. To the best of our knowledge, no research has been reported about this phenomenon in MAX phases. Generally, the shrinkage of unit cells occurs when small atoms are doped into their interstitial sites. The out-diffusion by a low melting point Si[21] and the weak Ti–Si bonding in Ti_3SiC_2 (ref. 22) may create Si vacancies. Hence, the unit cell of Ti_3SiC_2 could decrease because excess Si atoms may occupy the site of Si vacancies (inset of Fig. 4).

The densities of the products are shown in Fig. 5(a), and that of TS1.6C was the highest; TS1.2C (4.134 g cm^{-3}), TS1.4C (4.115 g cm^{-3}), and TS1.6C (4.151 g cm^{-3}). These values were lower than the theoretical value (4.50 g cm^{-3}) of Ti_3SiC_2,[13] while higher than those (3.792–3.836 g cm^{-3}) of our previous reports obtained by an arc melting process.[19] Fig. 5(b) shows the thermoelectric properties of TS1.2C, TS1.4C, and TS1.6C in the temperature range of ~590 °C. The electrical conductivity of TS1.2C (1.564×10^6/Ωm) was the lowest at room temperature, while those of TS1.4C (2.012×10^6 Ω^{-1} m^{-1}) and TS1.6C (1.995×10^6 Ω^{-1} m^{-1}) were similar. This result may be due to the different electrical resistivities of secondary phases such as TiC (70 μΩ cm)[23] and $TiSi_2$ (10 μΩ cm).[24,25] As can be seen in Fig. 3, the XRD intensities of TiC_x and $TiSi_2$ phases gradually decreased and increased, respectively, with increasing Si contents. When $TiSi_2$ phases with low resistivity compared with TiC_x phases were formed, the electrical conductivities of the products were improved. When the temperature was increased,

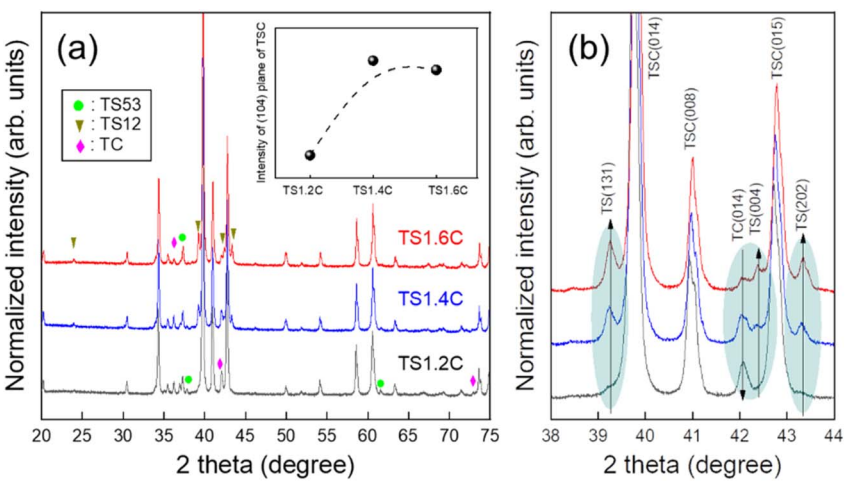

Fig. 3 (a) The whole and (b) enlarged XRD patterns of TS1.2C, TS1.4C, and TS1.6C.

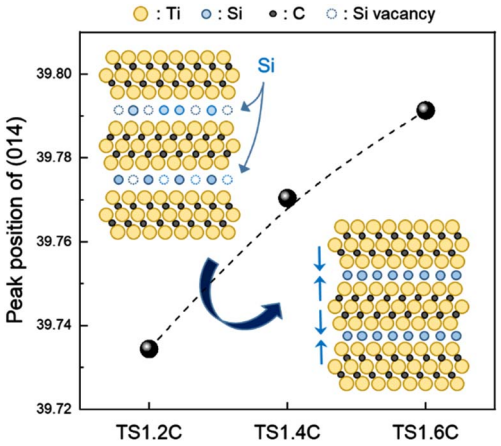

Fig. 4 The change of XRD peak positions of TS1.2C, TS1.4C, and TS1.6C.

their electrical conductivities gradually decreased: TS1.2C ($6.274 \times 10^5\ \Omega^{-1}\ m^{-1}$), TS1.4C ($7.814 \times 10^5\ \Omega^{-1}\ m^{-1}$), and TS1.6C ($7.532 \times 10^5\ \Omega^{-1}\ m^{-1}$) at 590 °C. This presents that the products have temperature-dependent behavior of metals. In general, a thermoelectric ZT value is used to present the performance of thermoelectric materials: $ZT = \alpha^2 T\sigma/\kappa$ (α, Seebeck coefficient; T, absolute temperature; σ, electrical conductivity; κ, thermal conductivity). This equation shows that the electrical and thermal conductivities are inversely proportional to each other. The Seebeck coefficients of TS1.2C, TS1.4C, and TS1.6C are 6.422–10.981 $\mu V\ K^{-1}$, 6.277–9.643 $\mu V\ K^{-1}$, and 5.778–9.543 $\mu V\ K^{-1}$, respectively (inset of Fig. 5(b)). These values are negative in the temperature range of ~590 °C, which indicates that the products were n-type.

Conclusions

Eggshell membranes with a net-like shape were used as carbon sources for fabricating the Ti_3SiC_2 phase. After thermal treatment at 900 °C, they were pulverized and mixed with Ti and Si powders. The mixed powders were condensed by an SPS process. Ti_3SiC_2 phases were successfully fabricated by thermal annealing using a tube furnace at 1500 °C. When Si contents were increased, $TiSi_2$ and TiC_x phases were formed and disappeared, respectively. The peak shift of Ti_3SiC_2 phases to a higher angle was observed in XRD analyses. The electrical conductivities of TS1.2C, TS1.4C, and TS1.6C were 1.564×10^6 to $6.274 \times 10^5\ \Omega^{-1}\ m^{-1}$, 2.012×10^6 to $7.814 \times 10^6\ \Omega^{-1}\ m^{-1}$, and 1.995×10^6 to $7.532 \times 10^5\ \Omega^{-1}\ m^{-1}$, respectively. Their Seebeck coefficients were negative and inversely proportional to the electrical conductivities: TS1.2C (6.422–10.981 $\mu V\ K^{-1}$), TS1.4C (6.277–9.643 $\mu V\ K^{-1}$), and TS1.6C (5.778–9.543 $\mu V\ K^{-1}$).

Author contributions

C. Nou performed the fabrication and process of MAX phase and analyses of the products; B. G. Kim gave ideas for this study; B. G. Kim, S. Y. Suk, and S. M. Choi planned the experiment; B. G. Kim and S. M. Choi wrote the manuscript; All authors have given approval to the final version of the manuscript.

Conflicts of interest

There are no conflicts of interest to declare.

Acknowledgements

This research was supported by the Basic Science Research Program through the National Research Foundation of Korea (NRF), funded by the Ministry of Education (No. NRF-2018R1D1A1A02086218 and No. NRF-2022R1A2C1092054). This result was also supported by "Regional Innovation Strategy (RIS)" through the National Research Foundation of Korea, funded by the Ministry of Education (2021RIS-004). In addition, this research was supported by the Pioneer Research Center Program through the National Research Foundation of Korea, funded by the Ministry of Science, ICT & Future Planning (NRF2022M3C1A309198811). S.-M. Choi thanks the Cooperative Equipment Center at KOREATECH for assistance with SEM and XRD analysis.

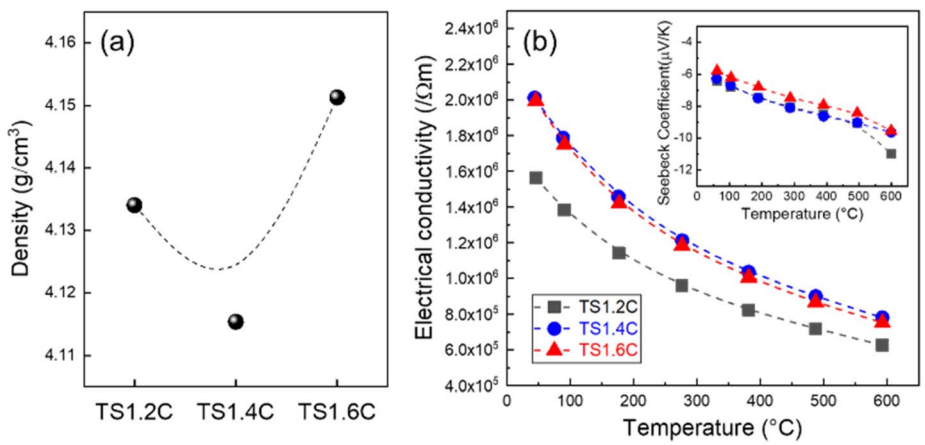

Fig. 5 (a) The densities, (b) electrical conductivities, and Seebeck coefficients (inset) of TS1.2C, TS1.4C, and TS1.6C.

References

1 M. Radovic and M. W. Barsoum, *Am. Ceram. Soc. Bull.*, 2013, **92**, 20–27.
2 M. W. Barsoum and M. Radovic, *Annu. Rev. Mater. Res.*, 2011, **41**, 195–227.
3 M. W. Barsoum and T. El-Raghy, *Am. Sci.*, 2001, **89**, 334–343.
4 B. Qiu, J. Wang, Y. Deng, M. Wang, Y. Wu and S. Z. Qiu, *Nucl. Eng. Technol.*, 2020, **52**, 1511–1520.
5 J. Xu, M.-Q. Zhao, Y. Wang, W. Yao, C. Chen, B. Anasori, *et al.*, *ACS Energy Lett.*, 2016, **1**, 1094–1099.
6 X. Liu, Q. Zhang, H. Zhang, Y. Jiang and Y. He, *J. Mater. Sci.*, 2016, **51**, 2594–2597.
7 Y. Gogotsi and B. Anasori, The rise of MXenes, *ACS Nano*, 2019, **13**, 8491–8494.
8 B. Anasori, M. Lukatskaya and Y. Gogotsi, *Nat. Rev. Mater.*, 2017, **2**, 16098.
9 M. Naguib, V. N. Mochalin, M. W. Barsoum and Y. Gogotsi, *Adv. Mater.*, 2014, **26**, 992–1005.
10 J. Pang, R. G. Mendes, A. Bachmatiuk, L. Zhao, H. Q. Ta, T. Gemming, *et al.*, *Chem. Soc. Rev.*, 2019, **48**, 72–133.
11 F. Sato, J.-F. Li and R. Watanabe, *Mater. Trans., JIM*, 2000, **41**, 605–608.
12 L. Yongming, P. Wei, L. Shuqin, C. Jian, W. Ruigang and L. Jianqiang, *Mater. Lett.*, 2002, **52**, 5245–5247.
13 N. F. Gao and Y. Miyamoto, *J. Mater. Sci.*, 1999, **34**, 4385–4392.
14 N. F. Gao, J. T. Li, D. Zhang and Y. Miyamoto, *J. Eur. Ceram.*, 2002, **22**, 2365–2370.
15 J. Wang, P. Nie, B. Ding, S. Dong, X. Hao, H. Dou, *et al.*, *J. Mater. Chem. A*, 2017, **5**, 2411.
16 J. Deng, M. Li and Y. Wang, *Green Chem.*, 2016, **18**, 4824.
17 Z. Bi, Q. Kong, Y. Cao, G. Sun, F. Su and X. Wei, *J. Mater. Chem. A*, 2019, **7**, 16028.
18 X. Zhang, M. Jiang, N. Niu, Z. Chen, S. Li, S. Liu, *et al.*, *ChemSusChem*, 2018, **11**, 11–24.
19 B. G. Kim, C. Nou, S. H. Bae and S.-M. Choi, *Ceramurgia Int.*, 2021, **47**, 17471–17475.
20 K. Buchholt, P. Eklund, J. Jensen, J. Lu, A. L. Spetz and L. Hultman, *Scr. Mater.*, 2011, **64**, 1141–1144.
21 H. Foratirad, H. Baharvandi and M. G. Maraghe, *J. Eur. Ceram. Soc.*, 2017, **37**, 451–457.
22 M. W. Barasoum, T. El-Raghy, C. J. Rawn, W. D. Porter, H. Wang, E. A. Payzant and C. R. Hubbard, *J. Phys. Chem.*, 1999, **60**, 429–439.
23 A. Z. A. Djafer, N. Saoula, N. Madaoui and A. Zerizer, *Appl. Surf. Sci.*, 2014, **312**, 57–62.
24 S. P. Murarka, D. B. Fraser, A. K. Sinha and H. J. Levinstein, *IEEE Trans. Electron Devices*, 1980, **27**, 1409.
25 J. Chen, J. P. Colinge, D. Flandre, R. Gillon, J. P. Raskin and D. Vanhoenacker, *J. Electrochem. Soc.*, 1997, **144**, 2437.